

# Fiber spectral domain optical coherence tomography for in-vivo rat brain imaging

Y. Xie<sup>1,2,\*</sup>, T. Bonin<sup>3</sup>, S. Loeffler<sup>4</sup>, G. Huettmann<sup>3</sup>, V. Tronnier<sup>5</sup>, U. G. Hofmann<sup>1,2</sup>

<sup>1</sup>Institute for Signal Processing, University of Luebeck, Luebeck, Germany

<sup>2</sup>Graduate School for Computing in Medicine and Life Sciences, University of Luebeck, Luebeck, Germany

<sup>3</sup>Institute for BioMedical Optics, University of Luebeck, Luebeck, Germany

<sup>4</sup>Clinic for Neurology, University Medical Center Schleswig-Holstein, Campus Luebeck, Germany

<sup>5</sup>Clinic for Neurosurgery, University Medical Center Schleswig-Holstein, Campus Luebeck, Germany

## ABSTRACT

A well established navigation method is one of the key conditions for successful brain surgery: It should be accurate, safe and online operable. Recent research shows that Optical Coherence Tomography is a potential solution for this application by providing a high resolution and small probe dimension. In this study a fiber Spectral-Domain OCT system with a super luminescent diode with the center wavelength of 840 nm providing 13.6  $\mu\text{m}$  axial resolution was used. A single mode fiber ( $\varnothing$  125  $\mu\text{m}$ ) was employed as the detecting probe. The information acquired by OCT was reconstructed into grayscale images by vertically aligning several A-scans from the same trajectory with different depth, i.e. forward scanning. For scans of typical white matter, the images showed a higher reflection of light intensity with lower penetration depth as well as a steeper attenuation rate compared to the scans typical for grey matter. Since the axial resolution of this OCT system is very high, some microstructures lying on the striatum, hippocampus and thalamic nucleus were visible in these images. The research explored the potential of OCT to be integrated into a stereotactic surgical robot as a multi-modal navigation method.

**Keywords:** Optical coherence tomography, fiber catheter, deep brain stimulation, Parkinson's disease, rat brain imaging

## 1. INTRODUCTION

Thanks to new techniques the human brain has over the last decades lost a lot of its complexity driven mystery and is thus now another organ to be subjected to surgical procedures and interventions. Prominent examples for these interventions are treatments for mental diseases and movement disorders which are based on electrical deep brain stimulation (DBS) [1, 2, 3, 4], stem cell therapy [5] or even micro lesioning [6, 7, 8]. As soon as the pathophysiological foundations of movement disorders such as Parkinson's disease were better understood, it was recognized that malfunctioning basal ganglia contribute to this syndrome, which made these deep brain structures one of the major targets for nowadays minimal invasive brain surgery. DBS in particular has been proven to be one of the most successful neurotherapies since its first application against Parkinson's symptoms and essential tremor in the 1990s [9].

One of the main parameters defining positive outcome of a stereotactic brain surgery is to precisely localize the target. MRT and CT are considered the standard image guidance systems for DBS [10, 11], but they do have disadvantages. Pre-operative images are obtained before the surgery and used for registration and navigation during the operation. Although the stereotactic frame and markers are placed on the skull to assist registration, errors can occur due to brain shift, lowering the accuracy of the planned trajectory and target. One solution is to use interventional MRI (iMRI) [12] to acquire real-time images and navigate during the surgery. However usual metal tools can't be used in iMRT guided surgery because of the high magnetic field (1.5 T) employed with the purpose of visualizing small targets; besides, an iMRI equipped operation room might not be an option for a research group due to high cost and space requirements. Our interest is to develop a real-time, low cost, portable navigation system for deep brain surgery, which is able to identify brain landmarks and compensate brain shift.

\* xie@isip.uni-luebeck.de; phone +49 451 5005809; fax +49 451 5005802;

Since the optical coherence tomography technology was demonstrated in 1991 by Huang et al. [13], it has developed rapidly in biomedical field. In general, OCT technology utilizes a low coherence interferometry to collect backscattered light from the object and obtain high resolution (up to 2  $\mu\text{m}$ ) [14, 15, 16, 17] volumetric tissue image in real time. Although the task of OCT imaging in high optically tissue is a challenge, there are many reports reveal its capability of imaging skin and vascular [18, 19]. One of the recent research highlight is OCT application in neural system, which includes visualizing architectural morphology of neural tissue and diagnosing neural disorders [20, 21, 22, 23]. The limitation of using OCT in brain imaging is that sufficient image contrast can be not easy to obtain, and speckle noise is proportional to tissue signal [24]. The penetration depth of OCT image rests with factors such as system sensitivity as well as tissue optical properties (absorption coefficient  $\mu_a$  and scattering coefficient  $\mu_s$ ). By taking the advantage of high sensitivity OCT system [25, 26], the image penetration depth around 0.5 to 1 mm in mammalian brain tissue [27, 28] and up to 2 to 3 mm in other tissue [29, 30] can be achieved. In particular, OCT can be combined with fiber optical technology to generate an endoscopic device with small dimensional flexible fiber based probe for intracavity or minimal-invasive imaging. Thus OCT has the potential to become an on-line navigation method for deep brain surgery [28, 31, 32, 33]

Current aim of our research is to develop a novel multi-modal navigation method using an integrated system [34] that includes OCT imaging and electrophysiology recording/navigation. In that context, we investigated whether fiber OCT could be used to differentiate brain gray matter from white matter and to identify characteristic brain structures as landmarks. A new approach was invented to reduce speckle noise in the image, which consequently enhanced image contrast.

## 2. MATERIALS AND METHODS

### 2.1 Spherical Assistant for Stereotactic SURgery (SASSU)

We used a commercial stereotactic surgical navigation frame (SASSU, pro-medTEC GmbH, Lübeck), which provides 5DOF (degrees of freedom) to place tools up to 200g of weight at any desired orientation within a planed position. Each of the five independent axes are individually equipped with a stepper motor (Nanote Electronic GmbH, Germany), providing a step motion resolution approximate to 1  $\mu\text{m}$  [35]. In order to improve location precision, each joint is integrated with an optical encoder. The whole system has a mechanical accuracy of ca. 30  $\mu\text{m}$  [35] and is run by a JAVA-based operation software. The software framework can adapt to most of the experimental strategies as it is complemented with several modules for planning, registration, and programmable surgical tool motion.

### 2.2 Optical Coherence Tomography System

The image acquisition system (Figure 1) which is employed throughout our study is a commercially available spectral radar OCT system ('Callisto', Thorlabs HL AG, Luebeck, Germany). A superluminescent diode (SLD) centered at 840 nm with a full-width-half-maximum of 44 nm is used as a light source. The axial and transversal resolutions are 13.6  $\mu\text{m}$  and 2.67  $\mu\text{m}$  in air, and the output power is 1.5 mW. In addition, the system has very high sensitivity at 100 dB and maximum SNR 80 dB. For the purpose of meeting varying refractive index of different tissue, we has developed a catheter accompany with an adjustable compensative reference setup. The light from the system is split into the sample arm and reference arm. In the reference arm, the light pass through a prism of which optical length is corresponded to the length of catheter then is reflected by a movable mirror. In the sample arm, the light passes through a fiber catheter and incident on the sample.

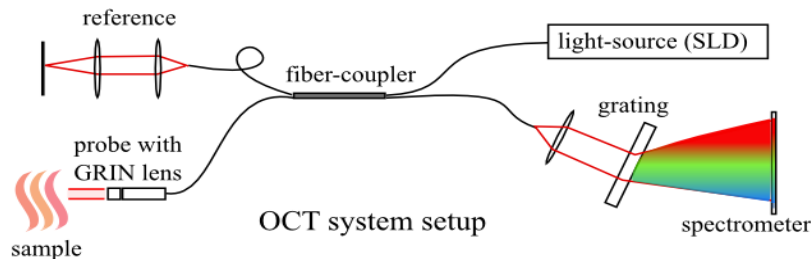


Figure 1. Schematic drawing of OCT system and the sketch of attached catheter probe.

The glass fiber catheter consists of a single-mode fiber running the length of the catheter and an optical focusing element at the end. The single-mode fiber is fused to a gradient-index (GRIN) lens. The quarter-wavelength pitch GRIN lens with

NA 0.2 is chosen to yield a required confocal parameter and spot size so that the penetrating depth is optimized when the catheter is inside of tissue. The full range of the A-scan is fixed at 2.7 mm optical depth with 512 pixels.

### 2.3 Surgical procedure

All experimental procedures performed were approved by the Ministry of Agriculture, Environment and Rural in Schleswig-Holstein State, and were consistent with the guidelines of the University of Luebeck Animal Welfare Office. The animals were fed regularly and housed in the University of Luebeck Animal Facility. All the experimental animals were adult Wistar rats (Centre d'élevage R. Janvier, Le Genest-St-Isle, France) weighed 350g-400g.

The rats were initially anesthetized by cocktail of 100mg/kg ketamine and 5mg/kg xylazine, administered by intraperitoneal injection, and given Acepromazin prior to the operation for pain management. The body temperature was maintained by a circulating water-bath heating pad which temperature was kept at 40°C. The rat was fixed onto a holding frame with a pair of ear pins and a tooth bar. The whole holding frame can be hooked to the SASSU platform (Figure 2). The hair was removed and the scalp was opened along the sagittal suture, the lesion was extended and fastened to the frame by suture threads. The rat was registered to the SASSU by using the explored skull landmarks Bregma, Lambda and sagittal suture. The skull target coordinate was marked by robotic assistant, and a small hole ( $\varnothing$  1mm) was drilled by a hand-held electric drill. The drilling was stopped before destroying the dura. During the whole experiment, the rat was given by 30% of the initial anesthesia dose when the rat showed toe-twitch reflex. Physiological saline was injected by subcutan administration in order to supplement body fluid.

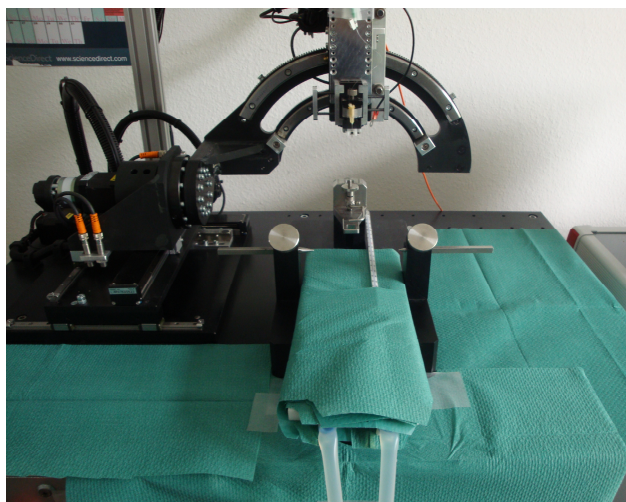


Figure 2. The surgical platform which is used in the experiment. The OCT probe is attached to the SASSU adaptor. The animal holding frame is fixed in the SASSU stage.

### 2.4 Measurement procedure

The optical fiber of the OCT was fixed to an adaptor mounted on the SASSU's semiarc arm. Prior to any measurement, the OCT system was calibrated to achieve the optimum contrast in the signal. The fiber probe was robotized positioned on top of the planed coordinate. The dura tissue was removed by fine tipped tweezer, before the fiber probe was inserted into the brain. The insertion procedure was monitored by OCT system, and the probe was manually triggered to step down until the brain surface was shown by the OCT signal to be in contact. With help of Thorlab's A-mode data streaming software and programmable SASSU motion, continuous probe insertion was synchronized with the data-stream of A-scans. The z-axis velocity of SASSU was set to 0.25 mm/s, with an initial acceleration at 3 mm/s<sup>2</sup>. The probe was manually stopped when the bottom of skull became visible in the data stream.

### 2.5 Tissue histology

Immediately after the experiment the rat was euthanized by carbon dioxide and the brain was removed from the skull. The tissue was fixated in 4% paraformaldehyde solution for about 24 hrs, and was then stored in 70% Ethanol. After fixation the brain was embedded in paraffin. The brain was sliced by a microtome with the tissue thickness set at around 8  $\mu$ m..

### 3. RESULTS AND DISCUSSIONS

Results shown originate from a trajectory starting on the rat skull at 4.1 mm posterior and 2.8 mm lateral to bregma (Figure 3). The information acquired by OCT system was reconstructed to be gray images by aligning vertical A-scans from the same trajectory with different depth. The scale of the gray value in the image indicated the intensity of backscattering light detected by the OCT system. A data streaming window with the A-scan sampling rate of 1.25 kHz was displayed online, which defined each A-scan column be acquired in 0.8 ms. While the fiber probe was inserted continuously at an axial speed of 0.25 mm/s, consecutive columns of the A-scan were taken 0.2  $\mu\text{m}$  deeper. The horizontal and vertical axis scales of the image were not geometric proportional. According to the OCT program settings each row of the data stands for 5.27  $\mu\text{m}$  depth.

The trajectory started from the brain surface and passed through the cortex (ctx), corpus callosum (cc) hippocampus (hipp), thalamic nucleus (th), and finally reached hypothalamic nucleus (hypo-th). Figure 3.left shows a coronal plane [36] of the rat brain section which were labeled by important structures, where the probe was inserted through. Figure 3.right shows the corresponding brain histology slice, the arrow indicates the initial entrance point of the trajectory.

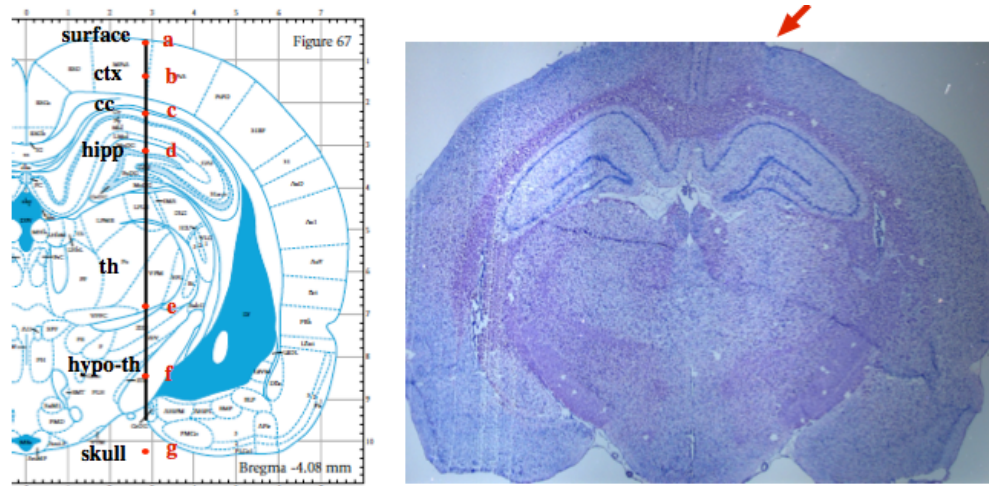


Figure3. Right shows the trajectory location, the markers show the recording data images which show in the next figure.  
Left is the histological slice of the trajectory region.

In imaging, we primarily related precisely measured location of the probe within the brain with structures found in a rat brain's atlas, which corresponded itself to the stained brain slices. The brain tissue can be generally separated into grey matter and white matter. Grey matter consists of neuronal cell bodies, neuropil, and glia cells, which is in contrast to white matter which contains mainly myelinated axon tracts. Grey matter is distributed in the outer part of cortex (neocortex) and deep nucleus; while the white matter is wrapped at the inner part of cortex and between the different deep nucleuses. Figure 4 shows the OCT images recorded during the probe insertion at different depth. The brain surface contact is shown in figure 4.a with a low penetrating depth. This is in contrast to the expected high penetration depth in the cortex, but can be explained by pronounced backscattering at the air / pia mater interface.

*Neocortex* is the outer part of cortex which consists of different dimension of the pyramidal cells and forms a six-layer structure. The cluster cell bodies contribute as the non-uniformities medium to a strong scattering of incident light, not only backscattering happens. Consequently the OCT signal in this region expresses a low intensity of backscattering light but a high penetrating depth (figure 4.b).

*Corpus callosum(cc)* is a thin layer around 0.3 mm thick between neocortex and hippocampus. It is the largest white matter structure in the brain, containing millions of axonal projections. The axon bundles are parallel aligned at Medial-Lateral direction, which is perpendicular to the OCT fiber trajectory. The axon is covered by a dense tissue called myelin sheath which is wrapped up in several layers. Aligned axon bundle together with myelin sheath contribute to strong backscattering tissue of light in near-IR spectrum (840 nm). Figure 4.c shows the ahead information when the probe was at the position 1.8 mm deep in the middle of corpus callosum layer. There is a distinct boundary which separates corpus callosum and the oriens layer of hippocampus. The high intensity block in the image is caused by the strong reflector

tissue axonal bundle in corpus callosum, while the weak intensity block in the image corresponds to the cell bodies layer in the hippocampus. The clearly visible border could be a landmark on entering hippocampus from the corpus callosum structure.

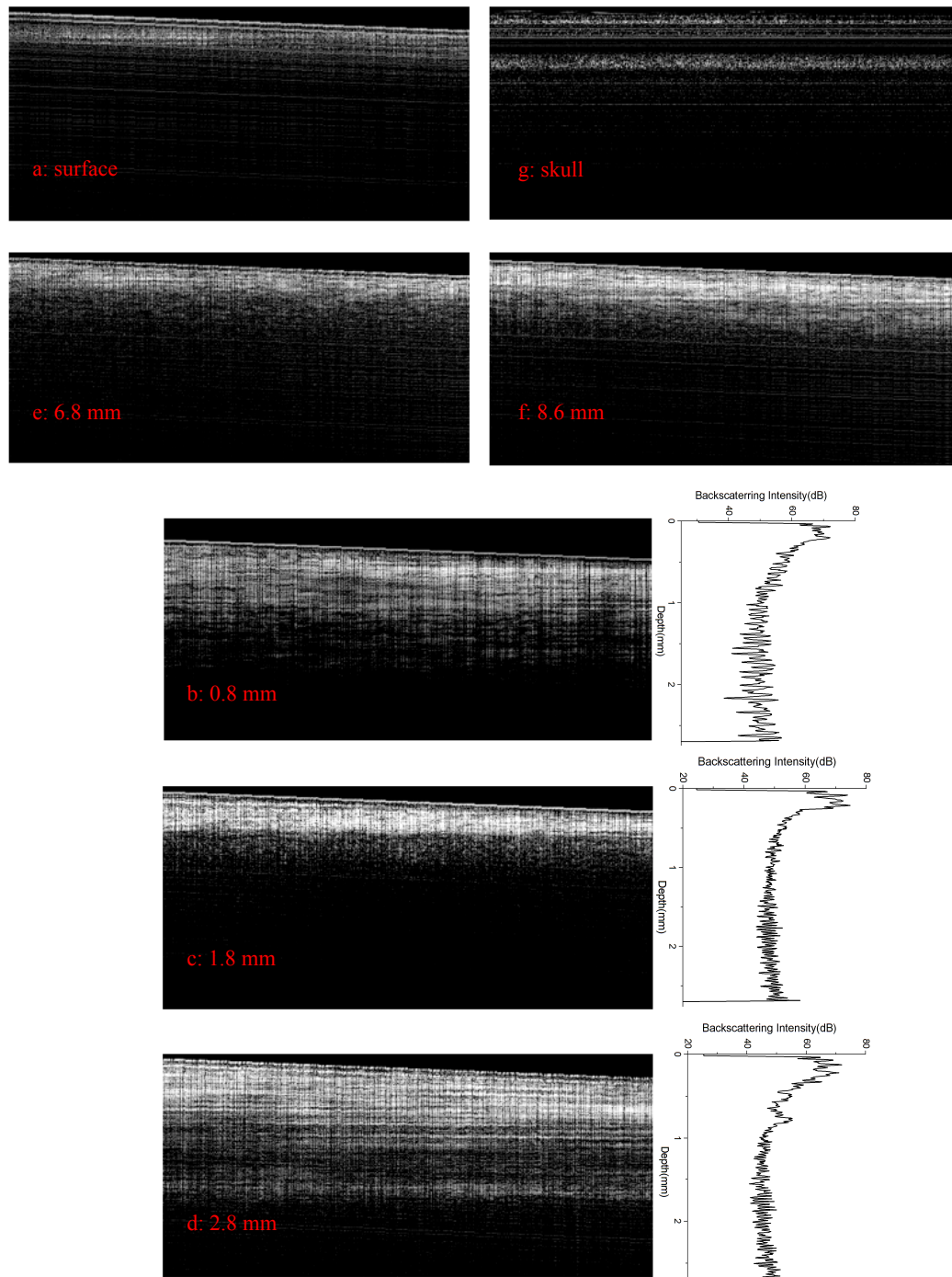


Figure 4. a) shows the brain surface when the probe was approaching the rat brain; b), c), d) are the images recorded in probe depth 0.8 mm (cortex), 1.8mm (corpus callosum) and 2.8mm (hippocampus), the plots indicates that the penetrating depth and the intensity are different in these regions; e), f) are the images obtained from thalamus and hypothalamus; g) shows the skull structure when the probe reached the bottom of the brain

*Hippocampus* is a piece of cortex folded onto itself in a peculiar shape. Many studies are focusing on understanding the mechanism of how it plays an important role in memory, emotion, and learning. Thus it is an important target in many brain surgeries and experiments. Figure 4.d shows the information from depth 2.8 mm in the hippocampus. The image performs a moderate level of light intensity and large penetration depth. When the probe was moved out of the hippocampus to the thalamus nucleus, a pair of highly contrasted structures appeared in the image.

*Thalamic nuclei* consist of a mixture of grey matter and white matter. The trajectory passed through lateral posterior thalamic nucleus (LPMR) and posterior thalamic nucleus (Po). The axon bundle direction in this region is not medial-lateral but dorsal-ventral. There is no clear difference or borders in these nucleus capsules, but the signal has the characters of low light intensity with low penetration depth, which is different in pure grey matter or white matter (Figure 4.e). This can be explained by containing axonal tracts among the bulk of cell bodies. In particular, the vertically aligned axon tracts do not contribute to high backscattered light, but disperse the incident light to the side. Thus it reduces the penetration depth compared to what is in pure grey matter.

*Hypothalamus* contains more than ten nuclei which play a role in neurosecretion. The OCT image (Figure 4.f) in this region shows a similar result as in the thalamus with no clear border among those nuclei capsules. The signal has an average light intensity of 70.21 and penetration depth at 0.45 mm. Anatomically, the hypothalamus is also a structure of mixed grey and white matter, resulting in no notable landmark between it and the thalamus. Different from the thalamus, the axonal tracts in hypothalamic nucleus have a varying orientations, most of which run in the caudal-rostral direction. For this reason, the incident light might be reflected by these myelinated axons so that appear a high intensity in the image.

We have made quantitative comparison of penetration depth and maximum light intensity between each homogeneous region of interests (ROI) in the OCT images. Results are shown in Table 1. They illustrate a strong difference in penetrating depth of brain structures, while the maximum backscattering intensity is of similar range.

Table 1. Penetrating depth and maximum intensity in brain structures

Brain structures	Penetrating depth	Maximum intensity
Cortex	0.50 mm	87.43
Corpus callosum	0.25 mm	90.72
Hippocampus	0.80 mm	81.95
Thalamus	0.30 mm	82.21
Hypothalamus	0.35 mm	84.46

Figure 5 shows a two-layer structure ahead. In Figure 5.left the second layer is displayed 0.65 mm in front of the probe, whereas the first layer is ahead (see arrows). The signal contrast is high enough to identify two layers ahead of the probe separated. This clearly shows the potential of the fibre OCT to find and display even small anatomical structures ahead of the probe.

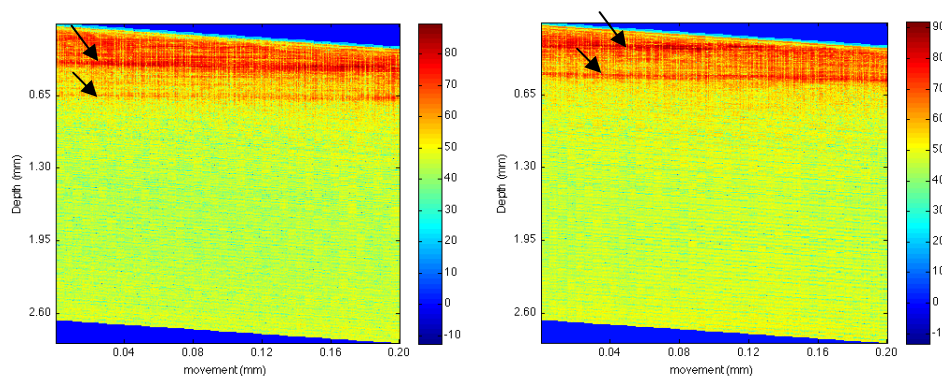


Figure 5. Color plots of two-layer structure, the interval of these two layers is 0.3 mm, and the thickness of each is 50  $\mu$ m.

#### 4. CONCLUSION

Our OCT system has its advantages in 1) high axial and transversal resolutions; 2) high sensitivity and good SNR; 3) small dimension of glass fiber catheter probe which can be used in minimum invasive surgery and 4) real time image acquisition algorithm.

In this study, we were able to differentiate main brain structures such as corpus callosum and hippocampus in living animal experiments on-line. Micro structures such as capsule boundaries and blood vessels are detectable in our system. We have demonstrated that fiber spectral OCT system may become an effective navigation modality to identify targets and localize surgical tools for brain interventions.

Since we had, besides the high precision control of the probe and an atlas, only post-mortem evidence for the anatomical area we took pictures in, we are working on an integrated system to obtain both OCT images and electrophysiology recordings during brain surgery [37]. This will enable us to determine our position by functional characteristic of the area, augmenting the knowledge of its position [38].

#### 5. ACKNOWLEDGEMENTS

Y.X. was supported by the Graduate School for Computing in Medicine and Life Sciences funded by Germany's Excellence Initiative [DFG GSC 235/1]. This project was supported by the German Research Ministry BMBF-grant 13N9190 "BiCIRTS".

#### REFERENCES

- [1] A. M. Lozano and N. Mahant, "Deep brain stimulation surgery for Parkinson's disease: mechanisms and consequences," *Parkinsonism & Related Disorders*. **10**, s49-s57 (2004)
- [2] C. Hamani, J. M. Schwalb, A. R. Rezai, J. O. Dostrovsky, K. D. Davis, and A. M. Lozano, "Deep brain stimulation for chronic neuropathic pain: Long-term outcome and the incidence of insertional effect," *Pain*, **125**, 188-196 (2006)
- [3] J. L. Ostrem and P. A. Starr, "Treatment of Dystonia with Deep Brain Stimulation," *Neurotherapeutics*. **5**, 320-330 (2008)
- [4] P. Gubellini, P. Salin, L. Kerkerian-Le Goff, and C. Baunez, "Deep brain stimulation in neurological diseases and experimental models: From molecule to complex behavior," *Progress in Neurobiology*. **89**, 79-123 (2009)
- [5] O. Lindvall, "Stem cells for cell therapy in Parkinson's disease," *Pharmacological Research*. **47**, 279-287 (2003)
- [6] F. A. Lenz, "Ablative surgery for the treatment of Parkinson's disease," *Handbook of Clinical Neurology*. **84**, 243-260 (2007)
- [7] K. Wester and E. Hauglie-Hanssen, "The prognostic value of intra-operative observations during thalamotomy for parkinsonian tremor," *Clinical Neurology and Neurosurgery*. **94**, 25-30 (1992)
- [8] M. I. Hariz, "Pallidotomy for Parkinson's Disease," *Encyclopedia of Movement Disorders*. 366-368 (2010)
- [9] A. L. Benabid, P. Pollak, D. Hoffmann, C. Gervason, M. Hommel, J. E. Perret, J. de Rougemont and D. M. Gao, "Long-term suppression of tremor by chronic stimulation of the ventral intermediate thalamic nucleus," *The Lancet*. **337**, 403-406(1991)
- [10] P. A. Starr, J. L. Vitek, M. DeLong, R. A. E. Bakay, "Magnetic Resonance Imaging-based Stereotactic Localization of the Globus Pallidus and Subthalamic Nucleus," *Neurosurgery*. **44(2)**, 303-313 (1999)
- [11] Jee-Young Lee, B. S. Jeon, Sun Ha Paek, Yong Hoon Lim, Mi-Ryoung Kim, and Cheolyoung Kim, "Reprogramming guided by the fused images of MRI and CT in subthalamic nucleus stimulation in Parkinson disease," *Clinical Neurology and Neurosurgery*. **112(1)**, 47-53 (2010)
- [12] P. A. Starr, A. J. Martin, and P. S. Larson, "Implantation of Deep Brain Stimulator Electrodes Using Interventional MRI," *Neurosurgery Clinics of North America*. **20(2)**, 207-217 (2009)
- [13] D. Huang, E. A. Swanson, C. P. Lin, J. S. Schuman, W. G. Stinson, W. Chang, M. R. Hee, T. Flotte, K. Gregory, C. A. Puliafito, and J. G. Fujimoto, "Optical coherence tomography," *Science*. **254**, 1178-1181 (1991)
- [14] T. A. Birks, W. J. Wadsworth, and P. S. J. Russell, "Supercontinuum generation in tapered fibers," *Opt. Lett.* **25**, 1415-1417 (2000)

- [15] K. Bizheva, B. Považay, B. Hermann, H. Sattmann, W. Drexler, M. Mei, R. Holzwarth, T. Hoelzenbein, V. Wacheck, and H. Pehamberger, "Compact, broad-bandwidth fiber laser for sub-2-μm axial resolution optical coherence tomography in the 1300-nm wavelength region," *Opt. Lett.* **28**, 707-709 (2003)
- [16] V. J. Srinivasan, M. Wojtkowski, J. G. Fujimoto, and J. S. Duker, "In vivo measurement of retinal physiology with high-speed ultrahigh-resolution optical coherence tomography," *Opt. Lett.* **31**, 2308-2310 (2006)
- [17] Y. Chen, S. W. Huang, A. D. Aguirre, and J. G. Fujimoto, "High-resolution line-scanning optical coherence microscopy," *Opt. Lett.* **32**, 1971-1973 (2007)
- [18] N. D. Gladkova, G. A. Petrova, N. K. Nikulin, S. G. Radenska-Lopovok, L. B. Snopova, Yu. P. Chumakov, V. A. Nasonova, V. M. Gelikonov, G. V. Gelikonov, R. V. Kuranov, A. M. Sergeev, and F. I. Feldchtein, "In vivo optical coherence tomography imaging of human skin: norm and pathology," *Skin Research and Technology* **6(1)**, 6-16 (2000)
- [19] F. J. van der Meer, D. J. Faber, I. Cilesiz, M. J. C. van Gemert, and T. G. van Leeuwen, "Temperature-dependent optical properties of individual vascular wall components measured by optical coherence tomography," *J. Biomed. Opt.* **11**, 041120 (2006)
- [20] S. A. Boppart, B. E. Bouma, M. E. Brezinski, G. J. Tearney, and J. G. Fujimoto, "Imaging developing neural morphology using optical coherence tomography," *J Neurosci Methods* **70(1)**, 65-72 (1996)
- [21] S. A. Boppart, M. E. Brezinski, B. E. Bouma, G. J. Tearney, and J. G. Fujimoto, "Investigation of developing embryonic morphology using optical coherence tomography," *Dev Biol.* **177(1)**, 54-63(1996)
- [22] S. A. Boppart, "Optical coherence tomography: Technology and applications for neuroimaging," *Psychophysiology*. **40(4)**, 529-541(2003)
- [23] M. S. Jafri, S. Farhang, R. S. Tang, N. Desai, P. I. S. Fishman, R. G. Rohwer, Cha-Min Tang, and J. M. Schmitt, "Optical coherence tomography in the diagnosis and treatment of neurological disorders," *J. Biomed. Opt.* **10**, 051603 (2005)
- [24] A. D. Mehta, J. C. Jung, B. A. Flusberg, and M. J. Schnitzer, "Fiber optic in vivo imaging in the mammalian nervous system," *Curr Opin Neurobiol.* **14(5)**, 617-28 (2004)
- [25] M. Choma, M. Sarunic, C. Yang, and J. Izatt, "Sensitivity advantage of swept source and Fourier domain optical coherence tomography," *Opt. Express*. **11**, 2183-2189 (2003)
- [26] S. (A. ) Yun, "Advances in Optical Coherence Tomography: Frequency Domain Technology and Applications," in Conference on Lasers and Electro-Optics/Quantum Electronics and Laser Science Conference and Photonic Applications Systems Technologies, OSA Technical Digest Series (CD) (Optical Society of America, 2007), paper CFL3
- [27] R. U. Maheswari, H. Takaoka, H. Kadono, R. Homma, and M. Tanifugi, "Novel functional imaging technique from brain surface with optical coherence tomography enabling visualization of depth resolved functional structure in vivo," *Journal of Neuroscience Methods*. **124(1)**, 83-92(2003)
- [28] K. Bizheva, A. Unterhuber, B. Hermann, B. Povazay, H. Sattmann, A. F. Fercher, W. Drexler, M. Preusser, H. Budka, A. Stingl, and T. Le, "Imaging ex vivo healthy and pathological human brain tissue with ultra-high-resolution optical coherence tomography," *J. Biomed. Opt.* **10**, 011006 (2005)
- [29] G. J. Tearney, M. E. Brezinski, B. E. Bouma, S. A. Boppart, C. Pitris, J. F. Southern, and J. G. Fujimoto, "In Vivo Endoscopic Optical Biopsy with Optical Coherence Tomography," *Science*. **276**, 2037-2039 (1997)
- [30] J. G. Fujimoto, "Optical coherence tomography for ultrahigh resolution in vivo imaging," *Nat biotchnol.* **21**, 1361-1367 (2003)
- [31] S. W. Jeon, M. A. Shure, K. B. Baker, D. Huang, A. M. Rollins, A. Chahlavi, and A. R. Rezaia, "A feasibility study of optical coherence tomography for guiding deep brain probes," *J Neurosci Methods*. **154(1-2)**, 96-101 (2006)
- [32] J. D. Johansson, P. Blomstedt, N. Haj-Hosseini, T. Bergenheim, O. Eriksson, and K. Wårdell, "Combined diffuse light reflectance and electric impedance measurements for navigation aid in deep brain surgery," *Stereotactic and Functional Neurosurgery*. **87(2)**, 105-113 (2009)
- [33] M. S. Jafri, R. Tang, and Cha-Min Tang, "Optical coherence tomography guided neurosurgical procedures in small rodents," *J Neurosci Methods*. **176(2)**, 85-95 (2009)
- [34] K. Mankodiya, D. Krapohl, S. Hammad, Y. Xie, M. Klinger and U. G. Hofmann, "A simplified production method for multimode multisite neuroprobes," Intern'l Conference on Neural Engineering 2009, Antalya, Turkey
- [35] L. Ramrath, U. G. Hofmann, A. Schweikard, "A robotic assistant for stereotactic neurosurgery on small animals," *The International Journal of Medical Robotics and Computer Assisted Surgery*. **4**, 295-303(2008)
- [36] G. Paxinos, and C. Watson, "The Rat Brain in Stereotaxic Coordinates,Compact 5th ed," Academic Press, San Diego, 107 (1997)

- [37] D. Krapohl, T. Bonin, et al. "A new integrated optical and electrophysiological sensor," *Biomed. Technik /Biomedical Engineering*. **53**(Supp 1), 126-128(2008)
- [38] C. K. E. Moll, A. Struppner and A. K. Engel, "Intraoperative Mikroelektrodenableitungen in den Basalganglien des Menschen," *Neuroforum*. **1**, 11-20(2005)

7715 - 85 V. 4 (p.9 of 9) / Color: No / Format: A4 / Date: 2010-04-08 04:23:38 AM

SPIE USE:  DB Check,  Prod Check, Notes: